

Exhibition of the periodicity of Quantum Fourier Transformation in Nuclear Magnetic Resonance

Xinhua Peng¹, Xiwen Zhu^{1*}, Ximing Fang^{2,1}, Mang Feng¹, Xiaodong Yang¹, Maili Liu¹,
and Kelin Gao¹

¹*Laboratory of Magnetic Resonance and Molecular Physics,
Wuhan Institute of Physics and Mathematics, The Chinese Academy of Sciences,
Wuhan, 430071, People's Republic of China*

²*Department of Physics, Hunan Normal University, Changsha, 410081,
People's Republic of China*

Abstract

The remarkable capability of quantum Fourier transformation (QFT) to extract the periodicity of a given periodic function has been exhibited by using nuclear magnetic resonance (NMR) techniques. Two separate sets of experiments were performed. In a full QFT, the periodicity were validated with state tomography and fidelity measurements. For a simplified QFT, the three-qubit pseudo-pure state was created by introducing an additional observer spin, and the spectra recorded on the observer spin showed intuitively the power of QFT to find the periodicity. Experimentally realizing the QFT provides a critical step to implement the renowned Shor's quantum factoring algorithm and many other algorithms. Moreover, it can be applied to the

*Corresponding author. E-mail: xwzhu@wipm.whcnc.ac.cn; Fax: 0086-27-87885291.

study of quantum chaos and other quantum information processing.

PACS numbers: 03.67.-a, 03.67.Lx, 02.70.-c, 89.70.+c

The most striking discovery in quantum computation is that quantum computers can efficiently perform some tasks which are not feasible on a classical computer. For example, the most famous of the current quantum algorithms — Shor’s quantum factoring algorithm [1], can factor a number exponentially faster than the best known classical algorithms, which leads to the cracking the RSA encryption system [2]. However, the key to Shor’s algorithm rests in an essential way on the application of a suitable quantum Fourier transform to efficiently determine the periodicity of a given periodic function [3]. The QFT is the key ingredient for not only Shor’s algorithm but also many other interesting quantum algorithms, including Simon’s algorithm (Simon 1994) [4,5], Kitaev’s algorithm [6,7], the estimating arbitrary phase algorithm [6,8] and the ordering-finding algorithm [8] etc.. Moreover, the scheme of exploiting quantum computation to study quantum chaos proposed by Schack [9], Brun and Schack [10], are also based on the QFT.

For an arbitrary positive integer x , the QFT can be defined by a unitary transformation [11,12,3]

$$QFT : |x\rangle \rightarrow \frac{1}{\sqrt{N}} \sum_{y=0}^{N-1} e^{2\pi i xy/N} |y\rangle, \quad \text{for } x \in \{0, 1, 2, \dots, 2^n - 1\}, \quad (1)$$

where $N = 2^n$, with n being the qubit number. Recently the QFT have been realized on a three bit NMR quantum computer. However, the implementation of the QFT was performed on the thermal equilibrium state [13] so that the striking power of the extraction of a periodicity wasn’t exhibited from the experimental results.

Imagine an oracle that computes a function $f : Z_n \rightarrow Z_m$ that has an unknown period r ($1 \leq r \leq 2^n$):

$$f(x + mr) = f(x), \quad (2)$$

where m is any integer such that x and $x + mr$ lie in $\{0, 1, 2, \dots, 2^n - 1\}$. The goal is to find the period r of $f(x)$. Classically, this problem is hard, requiring $O(2^n)$ queries to hit two equal values with high probability [14]. But a quantum algorithm described as follows can find r in time $\text{poly}(n)$ [12,15].

Define a unitary transform U :

$$U|x\rangle|y\rangle \rightarrow |x\rangle|y \oplus f(x)\rangle, \quad (3)$$

where \oplus denotes addition modulo 2. One first initialize two registers to $|0\rangle|0\rangle$, then create an equal superposition $\frac{1}{\sqrt{2^n}} \sum_x |x\rangle$ in the first register (easily prepared by applying $H^{(n)}$). Owing to quantum parallelism, querying the oracle and applying U prepare the state

$$|f\rangle = \frac{1}{\sqrt{N}} \sum_{x=0}^{N-1} |x\rangle |f(x)\rangle. \quad (4)$$

By measuring the second register, the result $|f(x_0)\rangle$ for some $0 \leq x_0 \leq r-1$ is obtained. In the meantime, the first register is collapsed into the state

$$|\psi\rangle = \frac{1}{\sqrt{K}} \sum_{j=0}^{K-1} |x_0 + jr\rangle, \quad (5)$$

where $N-r \leq x_0 + (K-1)r \leq N$. The periodicity r is not explicitly exhibited due to the offset x_0 .

Applying QFT to the state $|\psi\rangle$, one gets

$$F|\psi\rangle = \frac{1}{\sqrt{r}} \sum_{j=0}^{r-1} e^{2\pi i \frac{x_0 j}{r}} \left| j \frac{N}{r} \right\rangle. \quad (6)$$

A value c is supposed to be obtained by measuring the register, where c is necessarily a multiple of N/r , i.e., $c/N = \lambda/r$, ($0 \leq \lambda < r$). If λ is fortuitously coprime to r , r can be determined by cancelling c/N down to an irreducible fraction. According to the prime number theorem [12,16,17], the probability that λ is coprime to r is at least $1/\log r$ which exceeds $1/\log N$. Hence repeating the above procedure $O(\log N)$ times one can succeed in determining r with any prescribed probability $1 - \epsilon$ as close to 1 as desired.

Another way of analyzing the distribution of outcomes obtained is to calculate the reduced density matrix for the first register and calculate the measurement statistics. As the NMR quantum computer is ensemble quantum computation, we can achieve the statistical results of the probability distribution of the final state. It can be seen from Eq. (5) and (6) that, the QFT transforms the input state with the period r into the output state with

the period $k = N/r$ containing r items due to the displacement invariance of the QFT. For example, if the 3-qubit state $|\psi\rangle$ in Eq. (5) input to QFT is of the form

$$|\psi\rangle = \frac{1}{2}(|0\rangle + |2\rangle + |4\rangle + |6\rangle) \quad (7)$$

or

$$|\psi\rangle = \frac{1}{2}(|1\rangle + |3\rangle + |5\rangle + |7\rangle), \quad (8)$$

the state periodicity should be $r = 2$. Applying the QFT, one gets

$$QFT : |\psi\rangle = \frac{1}{\sqrt{2}}(|0\rangle + |4\rangle) \quad (9)$$

or

$$QFT : |\psi\rangle = \frac{1}{\sqrt{2}}(|0\rangle - |4\rangle). \quad (10)$$

From the state periodicity after the QFT $k = 4$ one can infer the state periodicity before the QFT $r = N/k = 2$, which is consistent with the state Eq. (7) or (8). Contrarily, if $|\psi\rangle$ has the form of Eq. (9) or (10), the state periodicity after the QFT $k = 2$ so that $r = N/k = 4$.

We have demonstrated these effects by liquid-state NMR using the carbon-13 labeled alanine $NH_3^+ - C^\alpha H(C^\beta H_2) - C' O_2^-$ dissolved in D_2O . All NMR experiments were performed on a Bruker ARX500 spectrometer with respect to transmitter frequencies of 500.13 MHz (1H) and 125.77 MHz (^{13}C). The measured NMR parameters are listed in Table 1. We can see from above that, the second register is only used to prepare the periodic state in the first register. Thus, in actual experiments, we just used the first register for determining the periodicity. In addition, owing to the nature of NMR ensemble, the display of the final state were performed by two different methods, tomography [22] and "spectral implementation" [23].

The logic network for the QFT is shown in Fig. 1 [8,11,18], consisting of a one-qubit gate

$$H_j = \frac{1}{\sqrt{2}} \begin{pmatrix} 1 & 1 \\ 1 & -1 \end{pmatrix}, \quad (11)$$

acting on qubit j and a controlled- R_d gate

$$R_d = \begin{pmatrix} 1 & 0 \\ 0 & e^{i\pi/2^d} \end{pmatrix} \quad (12)$$

acting on qubit j conditional on qubit k being in the $|1\rangle$ state with $d = j - k$. Here the H_j gate can be realized by the NMR pulse sequence $X_j(\pi)Y_j\left(\frac{\pi}{2}\right)$ or $Y_j\left(-\frac{\pi}{2}\right)X_j(\pi)$, and the controlled- R_j gate, by the pulse sequence $Z_j\left(\frac{\pi}{2}\right)Z_k\left(\frac{\pi}{2}\right)J_{jk}\left(-\frac{\pi}{2}\right)$ [19,20]. By carefully choosing the expressions for the Hadamard and Z gates and exploiting the commutation relations [21] to eliminate as many unnecessary operations as possible, the complete pulse for the QFT can be reduced as:

$$\begin{aligned} & X_1\left(-\frac{5\pi}{8}\right)Y_1\left(\frac{\pi}{2}\right)J_{21}\left(-\frac{\pi}{2}\right)J_{31}\left(-\frac{\pi}{4}\right)X_2\left(-\frac{\pi}{2}\right)Y_2\left(-\frac{\pi}{4}\right) \\ & X_2\left(-\frac{\pi}{4}\right)Y_2\left(\frac{\pi}{2}\right)J_{32}\left(-\frac{\pi}{2}\right)Y_3\left(-\frac{\pi}{2}\right)X_3\left(-\frac{5\pi}{8}\right) \end{aligned} \quad (13)$$

(applied from the left to the right). Finally a swap operation S_{13} are used to reverse the order of qubits to obtain the desired output from the QFT. We could just as easily relabel qubits 1, 2 and 3 in place of the Swap gate. Thus, we need not perform an actual physical swap gate here; a mental relabeling of the qubits is sufficient.

We performed two separate sets of experiments. In the first set, the full QFT was executed on a three-qubit quantum computer. Three ^{13}C nuclei were chosen as three qubits and protons were decoupled during the whole experiments by using a standard heteronuclear decoupling technique. All ^{13}C nuclei were taken 0.7ms for selective $\frac{\pi}{2}$ pulses of a *Gaussian* shape. At the beginning of the experiment, we labeled C' , C^α and C^β as spin 1, 2 and 3, respectively. After the QFT, we identify spin 1 with C^β spin 3 with C' .

The pseudo-pure state was prepared from the thermal equilibrium state by the procedure summarized in Table 2, in which the magnetic field gradients (denoted by G_z) to dephase off-diagonal elements of the density matrix at strategic points along the way were used [21]. Owing to the difference of the relaxation times between nuclei, we used a π rf pulse and a spell (the reversal recovery) to balance the effect of the different relaxation. Meanwhile step (1) in

Table 2 was replaced by the spell. By adjusting carefully the spell, the experimental spectra for a pseudo-pure state $\rho_{000} = I_1^\alpha I_2^\alpha I_3^\alpha (I_i^\alpha = |0\rangle\langle 0| = \frac{1}{2} + I_{iz})$ were finally recorded (shown in Fig. 2b) through reading-out pulses on the spectrometer. The normalized deviation density matrix ρ_{000} was confirmed by full tomography [22] shown in Fig. 3a.

The state in Eq. (7) and Eq. (9) can be prepared by the Hadamard gates $H_1 H_2$ and H_1 from the pseudo-pure state, respectively. Applying the sequence (13), the experimental spectra were shown in Fig. 2 (c) and (d). The density matrices were reconstructed from the obtained experimental spectra. The real parts of these matrices are shown in Fig. 3 (b) and (c), respectively. The fidelity of the QFT were calculated using the measure, called the *attenuated correlation* [24]

$$c(\hat{\rho}^{\text{exp}}) = \frac{\text{Tr}(\hat{\rho}^{\text{th}} \hat{\rho}^{\text{exp}})}{\text{Tr}(\hat{\rho}^{\text{th}} \hat{\rho}^{\text{th}})}. \quad (14)$$

Here, $\hat{\rho}^{\text{th}}$ is defined as a theoretical output state, transformed by the ideal transformation on a computer for the measured pseudo-pure state $\hat{\rho}_{000}^{\text{exp}}$, and an experimentally implemented control sequence for the same transformation on the spectrometer to get $\hat{\rho}^{\text{exp}}$. The values of the correlation for each of the three tomographic readouts were $c(\hat{\rho}_{000}^{\text{exp}}) = 1$ (by definition), $c(\hat{\rho}_{qft1}^{\text{exp}}) = 0.92$ and $c(\hat{\rho}_{qft2}^{\text{exp}}) = 0.84$. The measure reflects the imperfections of the experiments, including inhomogeneity of RF fields and static magnetic fields and imperfect calibration of rotations, gradient pulses and relaxation.

In the second set of experiments, we prepared a pseudo-pure state with introduction of an observer spin and employed a further simplification of the QFT proposed by Preskill [25], in which no two-qubit gates are needed at all and only n Hadamard gates and $n - 1$ single-qubit rotations are applied. Its key thoughts is the symmetry of the controlled- R_d gate on the two qubits, and to measure a single qubit first and then apply the controlled- R_d gate to the next qubit, conditioned on the outcome of the measurement of the qubit, instead of applying controlled- R_d and then measuring. Of course, it is only suitable for a special state, for example, the computational basis state $|x_3\rangle|x_2\rangle|x_1\rangle$, ($x_i = 0$ or 1) and the state in Eq. (7) and (9).

The pseudo-pure state $I_{0z}I_1^\alpha I_2^\alpha I_3^\alpha$ with introduction of an observer spin I_0 were prepared by a spatial averaging method proposed by Sakaguchi et al. [26], the procedure shown in Table 3. We chose C^α as the observer spin I_0 due to resolved scalar J couplings to all other spins and C' , C^β and H being joined directly with C^α as Spin 1 (I_1), 2 (I_2) and 3 (I_3), respectively. The methylic hydrogen nuclei were decoupled using the continuous wave (CW) mode.

The results of the second set of experiment were shown in Fig. 4. The transitions that connect the I_0^α and I_0^β manifolds of the observer spin I_0 are assigned to the computational basis states of the other spins. The readout on the observer spin I_0 can tell us which states the computational spins I_1 , I_2 and I_3 were in [23]. As exhibited in Fig. 4b, only one line corresponding to the $I_1^\alpha I_2^\alpha I_3^\alpha$ state indicated the computational spins I_1 , I_2 and I_3 was in the $|000\rangle$ state. It can be seen from Fig. 4c that, after swapping Spin 1 and Spin 3, I_1 , I_2 and I_3 was in $|000\rangle + |100\rangle = |0\rangle + |4\rangle$, thus the state periodicity $k = 4$ and the state periodicity before the QFT $r = N/k = 2$ was deduced; From Fig. 4d, I_1 , I_2 , I_3 was in $|000\rangle + |010\rangle + |100\rangle + |110\rangle$, hence, $k = 2$ and deduced $r = 4$. This simple readout method can make one quicker and more intuitive to get the results and is suitable for any number of qubits. Compared with the tomography [22] used in the first set of experiments, which is practically feasible for no more than three qubits, it is simpler and more efficient. However, its signal-to-noise ratio (SNR) is not very good and it is more demanding for the sample.

In conclusion, using the NMR techniques, the periodicity of the state can be extracted from the output state after applying the QFT, which exhibits the remarkable power of the QFT to determine the periodicity. Though the experimental imperfections cause the reduction of the fidelity, the powerful ability of quantum computers have been displayed. The QFT can be applied to many quantum algorithms and other quantum dynamics study. Recently, it has been used to implement the ordering-finding algorithm [27] and Shor's algorithm in NMR [28].

We thank Hanzheng Yuan, and Xu Zhang for help in the course of experiments.

REFERENCES

- [1] P. Shor, Algorithms for quantum computation: discrete logarithms and factoring. *Proc. of 35th Annu. Symp. on Found. of Computer Science*, (IEEE comp. Soc. Press, Los Alamitos, CA. 1994) 124-134.
- [2] R. L. Rivest, A. Shamir, and L. Adleman, *Comm. ACM* 21, 120 (1978).
- [3] M. A. Nielsen, & I. L. Chuang, *Quantum Computation and Quantum Information* (Cambridge Univ. Press, Cambridge, 2000).
- [4] D. Simon, 1994 *Proc. of 35th Annual Symposium on the Foundations of Computer Science*, p. 116. Los Alamitos, CA: IEEE Computer Society. (Extended abstract. Full version in 1997 *SIAM JI Comput.* 26.)
- [5] B. R. Jozsa, *Proc. R. Soc. Lond. A* **454**, 323 (1998).
- [6] A. Y. Kitaev, quant-ph/9511026.
- [7] D. S. Abrams and S. Lloyd, *Phys. Rev. Lett.* **83**(24), 5162 (1999)..
- [8] R. Cleve, A. Ekert, C. Macchiavello and M. Mosca, *Proc. R. Soc. Lond. A* **454**, 339-354, (1998).
- [9] R. Schack, *Phys. Rev. A* **57**, 1634 (1998)
- [10] T. A. Brun and R. Schack, *Phys. Rev. A* **59**, 2649 (1999).
- [11] D. Coppersmith, *An Approximate Fourier Transform Useful in Quantum Factoring* (IBM Res. Rep. RC19642, IBM T. J. Watson Research Centre, Yorktown Heights, New York, 1994)
- [12] A. Ekert, & R. Jozsa, *Rev. Mod. Phys.* **68**(3), 733 (1996).
- [13] Y. S. Weinstein, S. Lloyd and D. G. Cory, *Phys. Rev. Lett.* **86**, 1889 (2001).
- [14] D. K. Maslen and D. N. Rockmore, *Proc. DIMACS Workshop on Groups and*

Computation—II (1995).

- [15] A. Ekert, & R. Jozsa, *Phil. Trans. Roy. Soc. London Ser.A* **356**, 1769 (1998)
- [16] G. H. Hardy and E. M. Wright, *An introduction to the Theory of Numbers* (4th edition, Clarendon, Oxford, 1965).
- [17] M. R. Schroeder, *Number Theory in Science and Communication* (2nd enlarged edition, Springer, New York, 1990).
- [18] D. Beckman, A. N. Chari, S. Devabhaktuni, and J. Preskill, *Phys. Rev. A* **54**, 1034 (1996).
- [19] N. Gershenfeld, & I. L. Chuang, *Science* **275**, 350 (1997).
- [20] J. A. Jones, NMR quantum computation. *Prog. NMR Spectrosc.* **38**, 325 (2001).
- [21] R. Ernst, G. Bodenhausen and A. Wokaun, *Principles of Nuclear Magnetic Resonance in One and Two Dimensions* (Oxford Univ. Press, Oxford, 1990).
- [22] I. L. Chuang, N. Gershenfeld, M. Kubinec and D. Leung, *Proc. Roy. Soc. Lond A* **454**, 447 (1998).
- [23] Z. L. Madi, R. Bruschi and R. R. Ernst, *J. Chem. Phys.* **109**, 10603 (1998).
- [24] G. Teklemariam, E. M. Fortunato, M. A. Pravia, T. F. Havel and D. G. Cory, *Phys. Rev. Lett.* **86**, 5845 (2001).
- [25] J. Preskill, <http://www.theory.caltech.edu/~preskill/ph229>.
- [26] U. Sakaguchi, H. Ozawa, C. Amano, and T. Fukumi, *PRA* **60**, 1906 (1999).
- [27] L. M. K. Vandersypen, M. Steffen, G. Breyta, C. S. Yannoni, R. Cleve and I. L. Chuang, *Phys. Rev. Lett.* **85**, 5452 (2000).
- [28] L. M. K. Vandersypen, M. Steffen, G. Breyta, C. S. Yannoni, M. H. Sherwood and I. L. Chuang, *Nature* **414**, 883 (2001).

Table 1. Measured NMR parameters for alanine dissolved in D_2O on a Bruker ARX500 spectrometer.

nuclei	ν/Hz	$J_{C'}/Hz$	J_{C^α}/Hz	J_{C^β}/Hz	J_H/Hz
C'	-4320		34.94	-1.2	5.5
C^α	0	34.94		53.81	143.21
C^β	15793	-1.2	53.81		5.1
H	1550	5.5	143.21	5.5	

Table 2. The pulse sequence used to obtain the pseudo-pure state $\rho_{000} = I_1^\alpha I_2^\alpha I_3^\alpha$ from the thermal state, $\rho_{eq} = I_{1z} + I_{2z} + I_{3z}$. The refocusing π pulses were omitted during the evolution $\frac{1}{2J_{12}}$ due to $J_{13} \ll J_{12}$.

Pulse Sequence for $I_1^\alpha I_2^\alpha I_3^\alpha$	
(1)	$\left[\frac{\pi}{3}\right]_y^2 - \left[\frac{5\pi}{12}\right]_y^3 - G_z$
(2)	$\left[\frac{\pi}{2}\right]_x^1 - \frac{1}{2J_{12}} - \left[-\frac{\pi}{2}\right]_y^1 - G_z$
(3)	$\left[\frac{\pi}{4}\right]_x^2 - \frac{1}{4J_{23}} - [\pi]_x^1 - \frac{1}{4J_{23}} - \left[-\frac{\pi}{4}\right]_y^2 - G_z$
(4)	$\left[\frac{\pi}{4}\right]_x^1 - \frac{1}{2J_{12}} - \left[\frac{\pi}{4}\right]_y^1 - G_z$

Table 3 The pulse sequence for creating the labeled pseudo-pure state $\rho_{000} = I_{0z} I_1^\alpha I_2^\alpha I_3^\alpha$ from the thermal state, $\rho_{eq} = I_{0z} + I_{1z} + I_{2z} + I_{3z}$. The refocusing π pulses were omitted.

Pluse Sequence for $I_{0z} I_1^\alpha I_2^\alpha I_3^\alpha$	
(1)	$\left[\frac{\pi}{2}\right]_y^1 - \left[\frac{\pi}{2}\right]_y^2 - \left[\frac{\pi}{2}\right]_y^3 - G_z$
(2)	$\left[-\frac{\pi}{4}\right]_y^0 - \frac{1}{2J_{01}} - \left[-\frac{\pi}{4}\right]_x^0 - G_z$
(3)	$\left[-\frac{\pi}{4}\right]_y^0 - \frac{1}{2J_{02}} - \left[-\frac{\pi}{4}\right]_x^0 - G_z$
(4)	$\left[-\frac{\pi}{4}\right]_y^0 - \frac{1}{2J_{03}} - \left[-\frac{\pi}{4}\right]_x^0 - G_z$

Figure Captions

Fig.1 Efficient circuit for three qubit quantum Fourier transform. H represents the Hadamard gate and conditionality on a spin being in the $|1\rangle$ state is represented by a filled circle on its time line. The final symbol inside the box represents the swap S_{13} .

Fig.2 Experimental NMR spectra at different stages in the computation. (a) Experimentally measured thermal equilibrium spectra, acquired after a read-out pulse $\left(\frac{\pi}{2}\right)_y^i$ on spin i . (b) Experimental spectra for the pseudo-pure state $I_1^\alpha I_2^\alpha I_3^\alpha$. As desired, only one line is retained in each multiplet. (c) and (d) Output spectra of the QFT for the initial state $|\psi\rangle = |0\rangle + |2\rangle + |4\rangle + |6\rangle$ and $|0\rangle + |4\rangle$, respectively. The positive (negative) lines correspond to a spin in $|0\rangle$ ($|1\rangle$) before the readout pulse. The positive and negative lines counteract each other due to a spin in both $|0\rangle$ and $|1\rangle$, so that no line is retained on the spin. (c) and (d) have been magnified by a factor of two for clarity.

Fig.3 Experimental deviation density matrices: (a) for the pseudo-pure state $|000\rangle$, and for the states obtained after applying the QFT to the initial state $|\psi\rangle$ of, (b) $|0\rangle + |2\rangle + |4\rangle + |6\rangle$, and (c) $|0\rangle + |4\rangle$, respectively. The rows are enumerated in the standard computational basis. The left and right columns denote the real and imaginary components (in arbitrary units), respectively.

Fig.4 Experimental NMR spectra for the labeling spin I_0 at different stages during the computation. All spectra were recorded by a readout pulse $\pi/2$ on I_0 . (a) Experimentally measured thermal equilibrium spectra. (b) Experimental spectra for the pseudo-pure state $I_{0z} I_1^\alpha I_2^\alpha I_3^\alpha$. Only the transition $I_{0x} I_1^\alpha I_2^\alpha I_3^\alpha$ was presented, corresponding to the pure state $I_1^\alpha I_2^\alpha I_3^\alpha$. (c) and (d) Output spectra of the simplified QFT for the initial state $|\psi\rangle = |0\rangle + |2\rangle + |4\rangle + |6\rangle$ and $|0\rangle + |4\rangle$, respectively. The spectra of (b), (c) and (d) were added up 8 times by phase cycling, (c) and (d) were magnified by a factor of two and four for clarity, respectively.

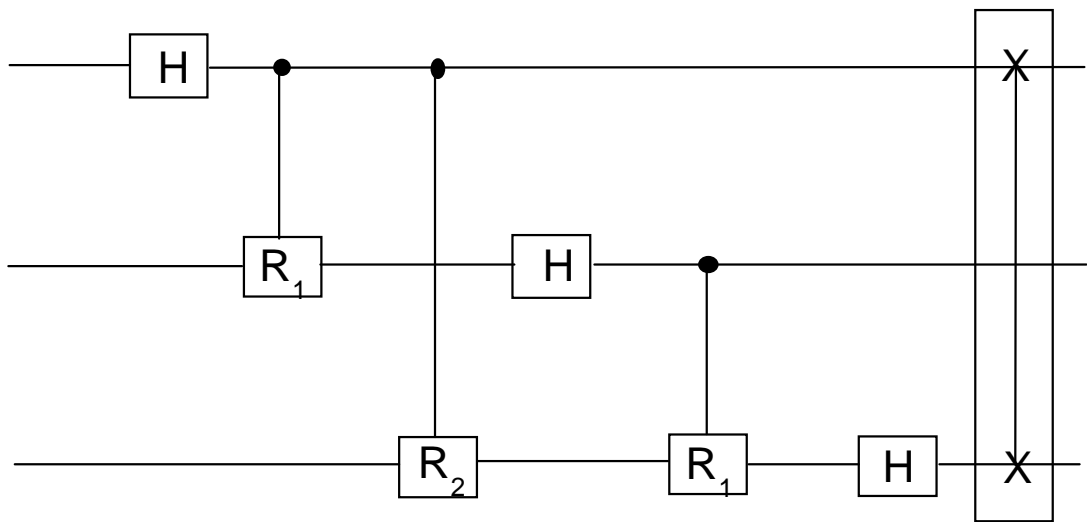


Fig. 1

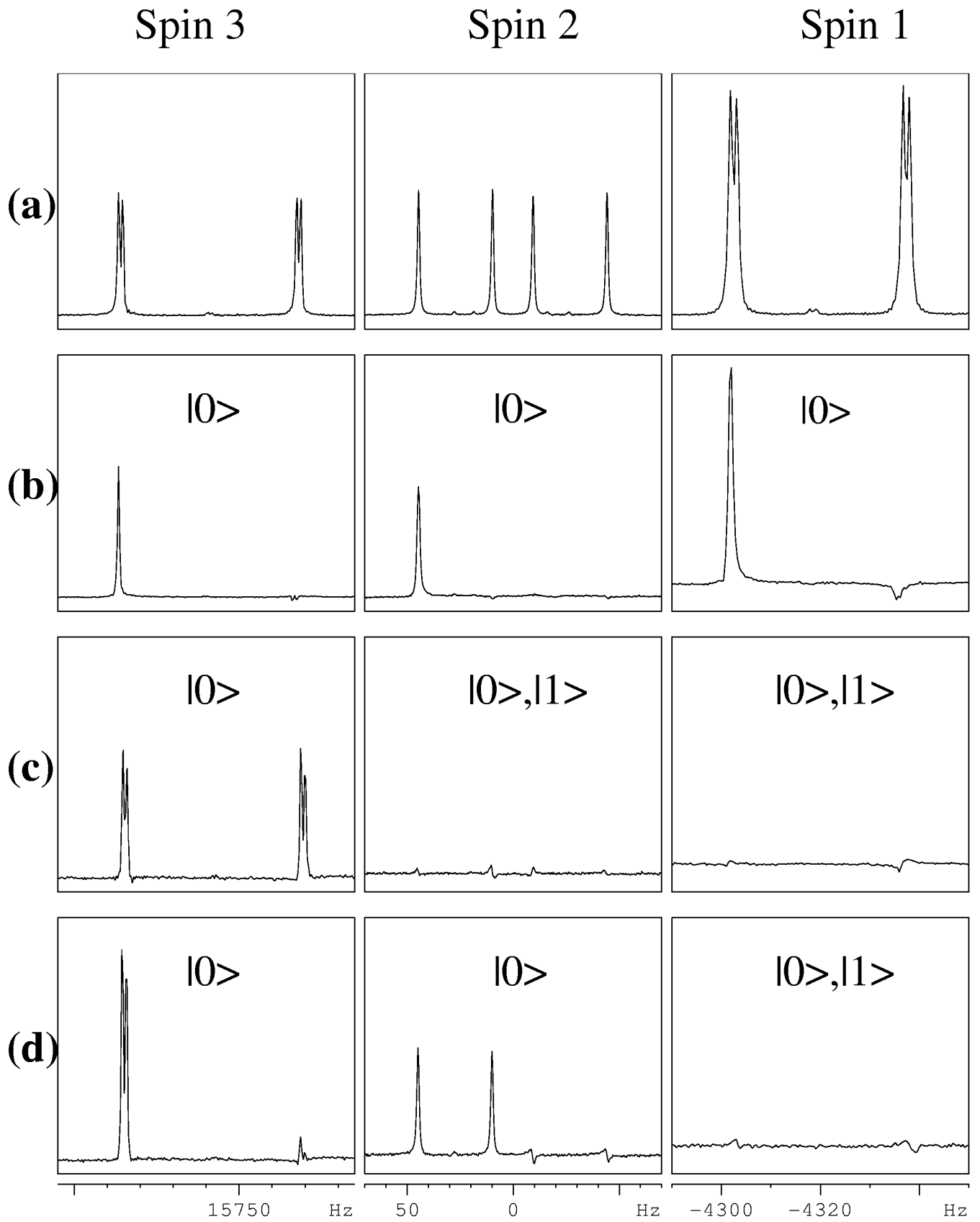


Fig. 2

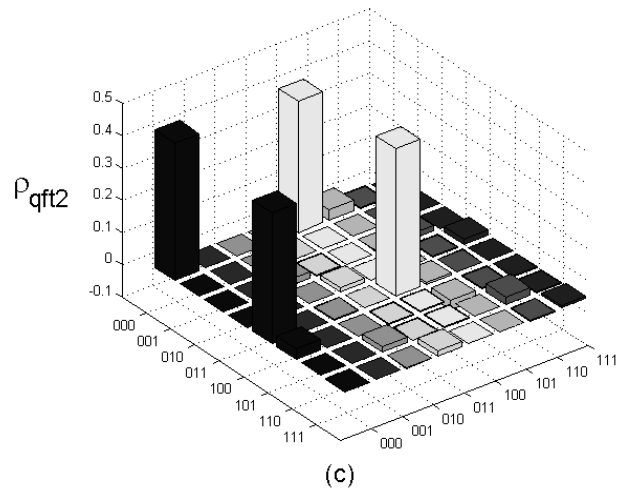
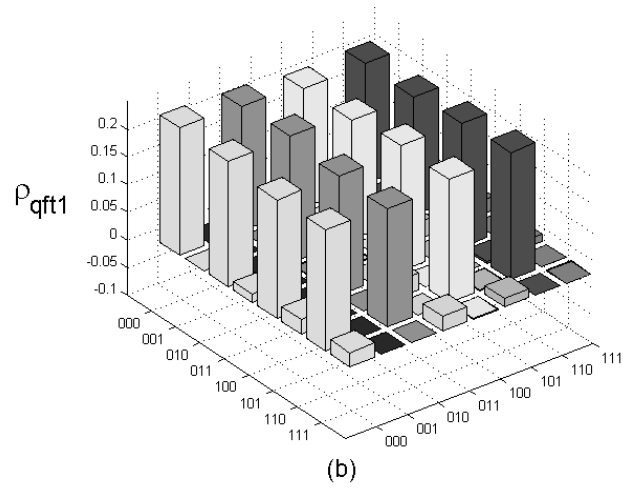
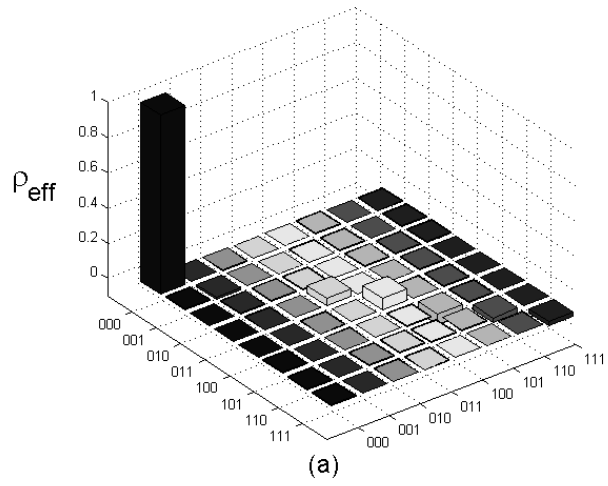


Fig. 3

Spin I_0

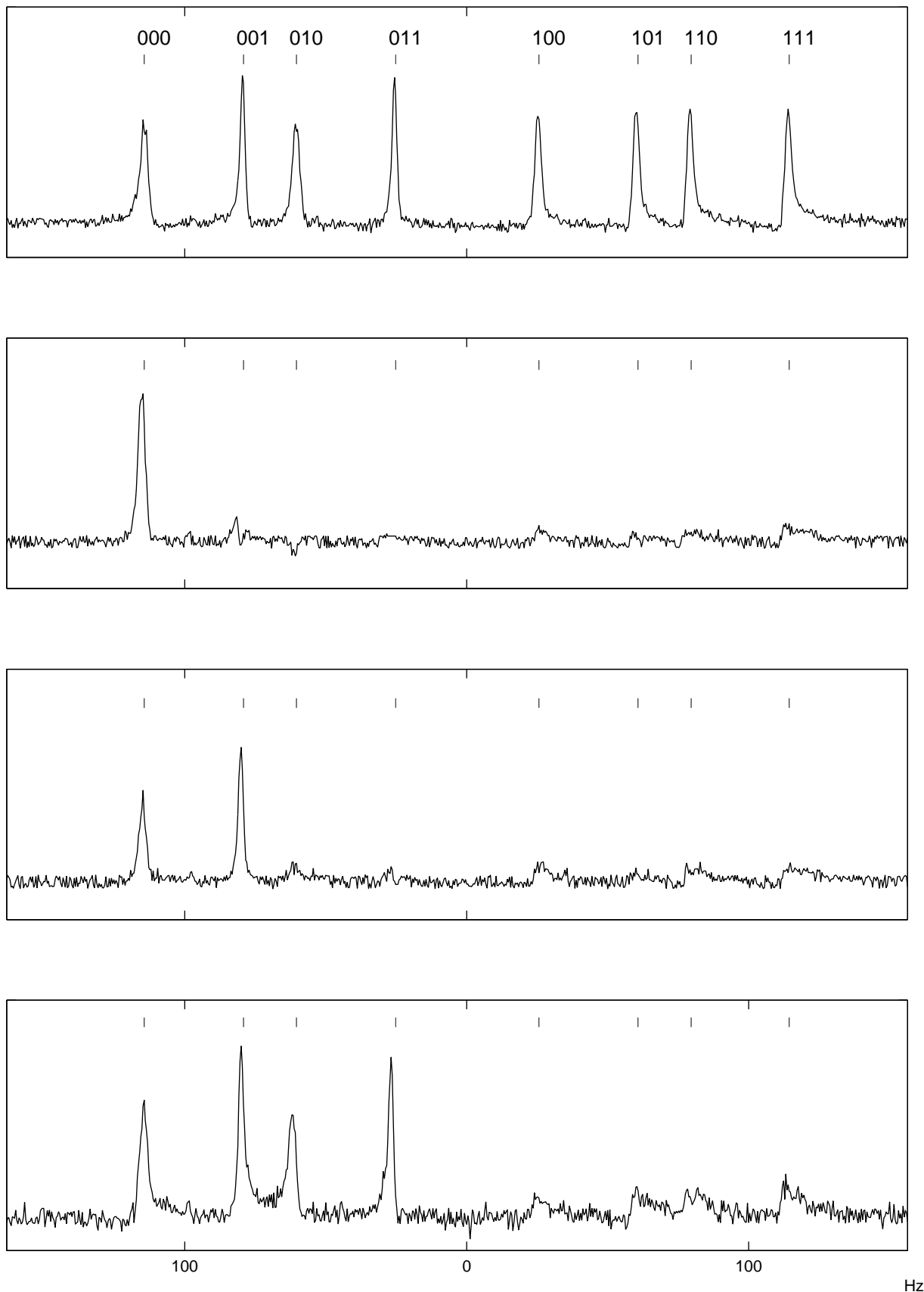


Fig. 4

Hz